Editorial

Fundus photography, fluorescein angiography, optical coherence tomography and electroretinography of preclinical animal models of ocular diseases

Sandeep Kumar^

Pharmaron (US) Lab Services, San Diego, CA, USA

Correspondence to: Sandeep Kumar. Director, Ophthalmology, Pharmaron (US) Lab Services, 7901 Vickers St., San Diego, CA 92111, USA.
Email: Sandeep.Kumar@pharmaron.com or sandymolbio@gmail.com.

Comment on: Xian B, Zhao M, Peng Y, *et al.* Fundus photography, fundus fluorescein angiography, and optical coherence tomography of healthy cynomolgus monkey, New Zealand rabbit, Sprague Dawley rat, and BALB/c mouse retinas. Ann Eye Sci 2023;8:10.

Keywords: Retinal fundus photography; sodium fluorescein and indocyanine green angiography; optical coherence tomography (OCT); electroretinography; animal models of ocular diseases

Received: 21 January 2023; Accepted: 01 March 2023; Published online: 24 March 2023.
doi: 10.21037/aes-23-6
View this article at: https://dx.doi.org/10.21037/aes-23-6

The eye is an immune-privileged and sensory organ in humans and animals. Anatomical, physiological, and pathobiological features share significant similarities across divergent species (1). Each compartment of the eye has a unique structure and function. The anterior and posterior compartments of the eye contain endothelium (cornea), epithelium (cornea, ciliary body, iris), muscle (ciliary body), vitreous and neuronal (retina) tissues, which make the eye suitable to evaluate efficacy and safety of tissue specific drugs (2). Certainly, it's critical to understand disease associated pathophysiology mechanisms and novel molecular pathways, to help develop novel therapeutics to improve current treatment strategies for eye diseases. However, to accomplish these objectives, a well-characterized and validated animal model of a disease is an absolute necessity. Transgenic and experimental animal models have provided remarkably reproducible systems to explore and characterize the key molecules involved in the etiology and pathogenesis of eye diseases. Furthermore, these models have provided platforms to evaluate the efficacy and dose responses of newly characterized pharmacological agents (3-6). Thus, the development and characterization of novel animal models in different species (rodents, rabbits, dogs, pigs, and non-human primates) is crucial for ocular drug development programs. Based on Food and Drug Administration (FDA) requirements, translational studies in preclinical ocular research must include *in vivo* assessments, such as assessment of structural and functional changes in the retina using optical coherence tomography (OCT) after a drug delivery. Traditionally, morphological changes have been evaluated by histological analysis, which necessitates sacrificing the animals. *In vivo* examination and imaging modalities like slit lamp imaging, indirect ophthalmoscopy, color fundus photography, sodium fluorescein (NaF) and indocyanine green (ICG) angiography (vasculature leakage), and spectral domain OCT (SD-OCT; *in vivo* histogram) allow noninvasive, non-contact, and rapid imaging of the posterior and anterior segments (AS) of the animal eye (*Figure 1*) (3-9). Furthermore, functional changes in the retina are evaluated using electroretinography (ERG; photoreceptor function) to track disease progression in animal models before and after treatment (10,11). Additional tools, such as optokinetic response (OKR), have been used to test visual acuity in rodent studies (12,13). In this *Annals of Eye Science* article,

^ ORCID: 0000-0002-2918-8276.

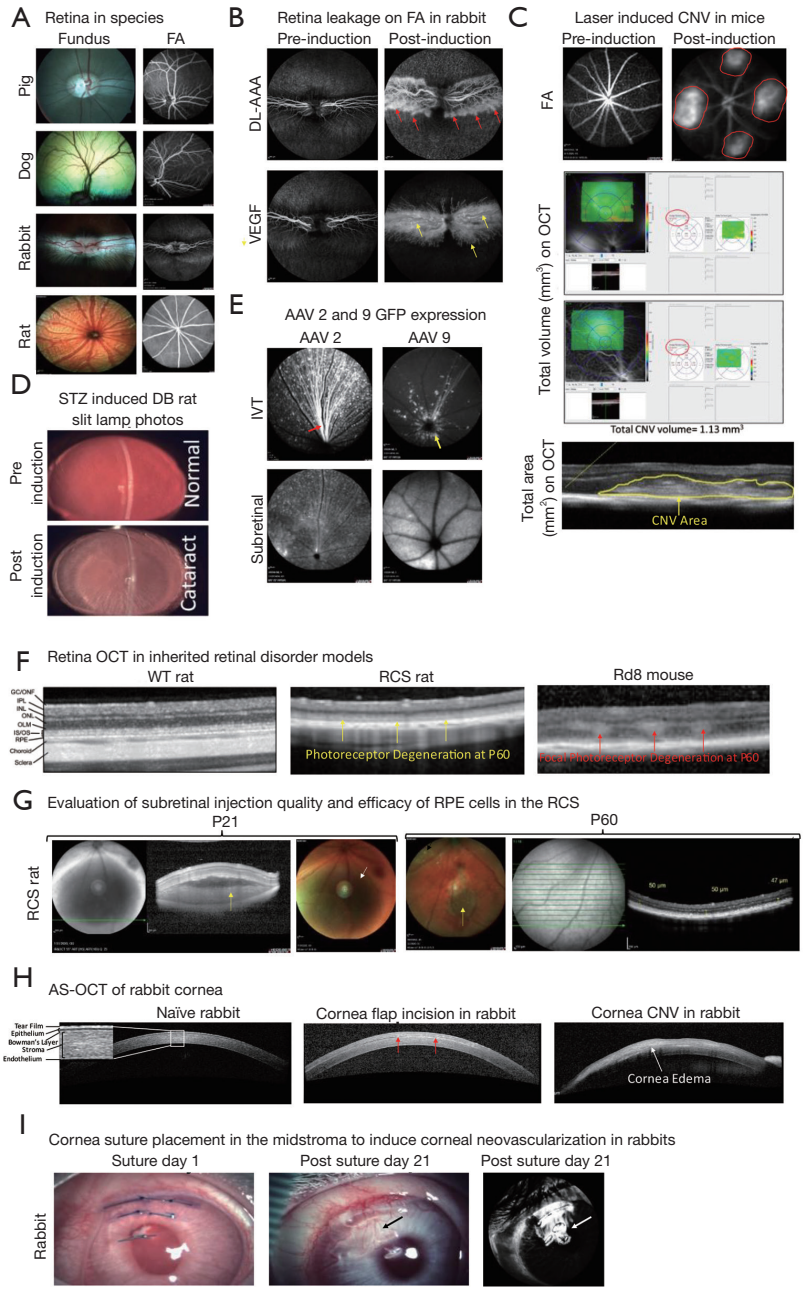

Figure 1 *In vivo* imaging techniques to assess anterior and posterior segment integrity in preclinical ocular animal models. (A) Retina vessels pattern in different species: representative images of color fundus photograph and FA of merangiotic (rabbit) and holangiotic (rat, pig and dog) retina. The glowing reflective lining in the dog retina fundus represents tapetum lucidum that is located between the retina and RPE. (B) FA in rabbit: development of retinal neovascularization (red arrows, top panel) on day 15 post DL-AAA induction in DB rabbit and vascular permeabilization on day 3 post VEGF induction, yellow arrows (bottom panel) indicate the leakage of NaF from primary, secondary and capillaries retinal vessels in DB rabbit. (C) Laser induced CNV in mouse: FA on day 7 post laser photocoagulation shows grown CNV and leakage from the CNV lesions (areas drawn in red, top panel). CNV volume analysis on day 7 using OCT (middle panel), total CNV volume = retinal thickness volume on day 7–retinal thickness volume on day 1. CNV area analysis on day 7 using OCT (area drawn in yellow, bottom panel). (D) Lens cataract evaluation by slit lamp photography: slit lamp imaging shows lens cataract formation in a diabetic rat, induced by IV injection of STZ, on day 35 post induction. (E) GFP expression following subretinal and IVT injection in mice:

representative Heidelberg Spectralis® images showing that IVT delivery of AAV serotype 2 efficiently transduce outer retinal cells (red arrow represents nerve fiver transduction) while AAV serotype 9 express GFP expression in the optic disc (yellow arrow). Subretinal delivery of AAV2 and 9 transduced photoreceptors (bottom panel). (F) Retina OCT in IRD animal models: retina OCT scan shows intact retinal layers at P days 60 in a naïve (WT) Sprague Dawley rat. Complete loss of ONL (represents health and integrity of photoreceptor cells) was seen in a P60 RCS rat (yellow arrows). A *rd8* mouse showing nasal focal retinal photoreceptor degeneration (red arrows) at P60. (G) Evaluation of subretinal injection quality and efficacy of RPE cells in the RCS rat: OCT and fundus images immediately post subretinal injection of RPE cells in RCS rat on P21 show successful delivery [yellow arrow on OCT represents RPE cells in the subretinal space, white arrow on fundus represents a bleb formation (hallmark for a successful subretinal injection)] post RPE cells injection into the subretinal space, note: no lens damage, retinal atrophy or retinal/vitreous hemorrhage present. P60 OCT scan shows rescue of the photoreceptor (preserved ONL). Yellow arrow on fundus image represents a small retinal scar formation at the injection site at P60. (H) AS OCT imaging in rabbit: AS-OCT scan in naïve rabbit showing the intact cornea layers. Middle panel shows cornea AS-OCT immediately after cornea flap surgery (red arrows). Far right OCT scan shows cornea edema in a suture induce corneal neovascularization in rabbits. (I) Cornea suture placement in the mid-stroma to induce corneal neovascularization in rabbits: full field slit lamp image showing suture placement in the stroma on day 1. Post suture placement on day 21, slit lamp image and anterior fluorescein angiogram show the grown cornea neovascularization (black and white arrows on slit lamp and anterior fluorescence angiogram, respectively). FA, fluorescein angiography; DL-AAA, DL-2-aminoadipic acid; VEGF, vascular endothelial growth factor; CNV, choroidal neovascularization; OCT, optical coherence tomography; STZ, streptozotocin; DB, Dutch Belted; AAV, adeno-associated viruses; GFP, green fluorescent protein; IVT, intravitreal; WT, naïve animal; RCS, Royal College of Surgeons; rd8, retinal degeneration 8; IPL, inner plexiform layer; INL, inner nuclear layer; ONL, outer nuclear layer; OLM, outer limiting membrane; IS/OS, inner and outer segment; RPE, retinal pigment epithelium; P, postnatal; AS, anterior segment; NaF, sodium fluorescein; IV, intravenous; IRD, inherited retinal disorder.

Xian *et al.* (14), have comprehensively examined and discussed the normal anatomical structures of healthy experimental animals like cynomolgus monkeys, New Zealand rabbits, Sprague Dawley rats, and BALB/c mice. In this editorial section, more emphasis is placed on the implications of *in vivo* imaging to characterize disease phenotypes in different ocular preclinical animal models, involving the anterior and posterior compartments of the eye.

Animal species for ocular preclinical studies

Rodents are commonly used for proof-of-concept studies due to their small size, ease of maintenance, short life cycle, cost effective and abundant genetic resources. Because of the abundance of transgenic or knockout models, rodents are the preferred model for studying inherited retinal degenerative diseases like retinitis pigmentosa, Stargardt's disease, for cell and gene therapy products (3-6). Besides these fully characterized genetically modified rodent models, chemically or mechanically induced rodent models are also well established and widely used in basic and translational ocular research, including laser-induced choroidal neovascularization (CNV), streptozotocin (STZ)-induced diabetic retinopathy, sodium iodate or N-methyl-N-nitrosourea-induced photoreceptor degeneration, alcohol/alkali/cryo freeze corneal wound healing models, to name a few. In many of these rodent models, onset and progression of the disease are well defined. However, heterogeneity in the animal population and the smaller size of the eyes can make it challenging to perform some specialized injection techniques like subretinal, intravitreal or suprachoroidal.

In terms of size and physiology, rabbit eyes are very similar to human eyes. Accordingly, rabbit is the preferred choice to establish the safety and tolerability of ocular drugs and devices, but not for cell and gene therapy products due to the unavailability of transgenic or knockout models. In addition, large animals like dogs and pigs who have similar size to the human eye, are also ideal for the short- or long-term safety and tolerability evaluation of ocular drugs. These large species are lacking a macula, like humans or non-human primates, but have a similar cone rich region called the area centralis. Disease phenotypes in large animal species can also be induced either chemically or mechanically, for example, laser induced CNV, mechanical debridement of retinal pigment epithelium (RPE)/photoreceptor layer, keratitis (viral and bacterial) in rabbit, DL-2-aminoadipic acid (DL-AAA) or vascular endothelial growth factor (VEGF) induced retinopathy rabbit models, alcohol/alkali/cryo freeze corneal wound healing models in

rabbit/dogs/pigs etc. All these models are extensively used in preclinical ocular studies.

In vivo imaging techniques used to assess structural and functional changes in preclinical *in vivo* ocular models

Color fundus photography

Retinal color fundus photography is a noninvasive *in vivo* imaging procedure that utilizes specially designed cameras to photograph the animal's retina through dilated pupils (*Figure 1A* shows the funduscopic features in healthy animals of different species). Fundus examination and imaging is used to examine the clinical appearance of the retina, retina/choroid vasculature, neuronal fibers, and optic nerve morphology (15). The retinal fundus imaging technique allows longitudinal evaluation of disease progression as well as the efficacy and safety of ocular drugs in animal models. In animal disease models, the most common fundus features are: (I) tortuous and engorged retinal vessels (II) exudates from the leaky vessels (III) retinal or vitreous hemorrhage (IV) retinal degeneration; (V) retinal scar tissue; (VI) retinal/RPE/choroid areas of atrophy, (VII) vitreous floaters or posterior vitreous detachment. In preclinical animal studies, fundus photography is often combined with fluorescein angiography (FA) and ICG angiography (ICGA) to help interpret angiography features, since certain retinal landmarks visible in fundus photography are not visible on FA.

NaF and ICGA

FA and ICGA are used to image and evaluate the integrity of retinal and choroidal blood vessels, respectively, using high-resolution digital imaging systems or scanning laser ophthalmoscopes (SLO) together with infrared-sensitive video cameras. The NaF dye spectrum falls in the visible range (peak absorbance ~485 nm and peak emission ~525 nm) (15,16), which doesn't penetrate through the RPE and is therefore only considered good to image and evaluate the retinal vasculature's integrity. The infrared spectrum of ICG dye (the absorption spectrum ranges from 790 to 805 nm, while the emission spectrum ranges from 770 to 880 nm, with the peak emission at 835 nm) (17,18) allows visualization of the choroidal vasculature. FA is used to image the retinal vasculature, and in contrast, ICGA can be used to image both the retinal and choroidal vasculature. ICG has a higher serum protein-binding affinity in the blood vessels (98%) than NaF (75%), resulting in less extravasation of ICG through gap junctions and improved imaging of choroidal vasculature (16-19). Like in humans, NaF and ICG can be delivered alone or in combination intravenously to capture retinal or choroidal lesions during early, middle, and late phase of the angiograms in the animals (3,5,19). In preclinical animal models, like diabetic retinopathy, retinal vein occlusions, CNV due to age-related macular degeneration, corneal neovascularization, and others, FA or ICGA images are graded based on the attenuation of blood vessels, amount of NaF or ICG leakage from the vessels and location or type of lesion (*Figure 1B*,*1C*,*1I*). Angiograms are also useful for describing retinal or choroidal lesions based on the fluorescence in the lesion during the time course of angiography (3-5,20,21). In addition, the visible and infrared spectra of SLO are used to qualitatively analyze the expression of green fluorescent protein (GFP) and mCherry (red) proteins in live animals (*Figure 1E*).

OCT

OCT is a non-invasive, non-contact imaging technique, which produces high-resolution images of the posterior segment (RPE, choroid, retina, vitreous, and optic nerve) and AS (cornea, iridocorneal angle etc.) of the eye in different animal species. OCT provides useful insight on the progression of anterior/posterior segment-related diseases and quantitatively assesses and evaluates the efficacy and safety of a specific treatment over time (*Figure 1F*) (3-6). The posterior segment OCT scan contains sclera, choroid, RPE, inner segment and outer segment photoreceptor layers, outer and inner nuclear layers, outer and inner plexiform layers, nerve fibers, and ganglion cell layers (*Figure 1F*). The OCT machine's inbuilt software (for example, Heidelberg Spectralis® Eye Explorer (HEYEX) software in Heidelberg Spectralis® imaging system) can segment all retinal layers and perform individual layer thickness measurements; for example, measuring the outer nuclear layer in a photoreceptor degeneration model (*Figure 1G*). In addition, total volume OCT scans are useful to provide the total retinal volume (mm^3) or area (mm^2) of a selected area that is being set during the scan, for example, measurements of the CNV volume or total area measurement in a rodent laser-induced CNV model (*Figure 1C*). OCT imaging can be used to assess the quality of injection procedures like subretinal, intravitreal and

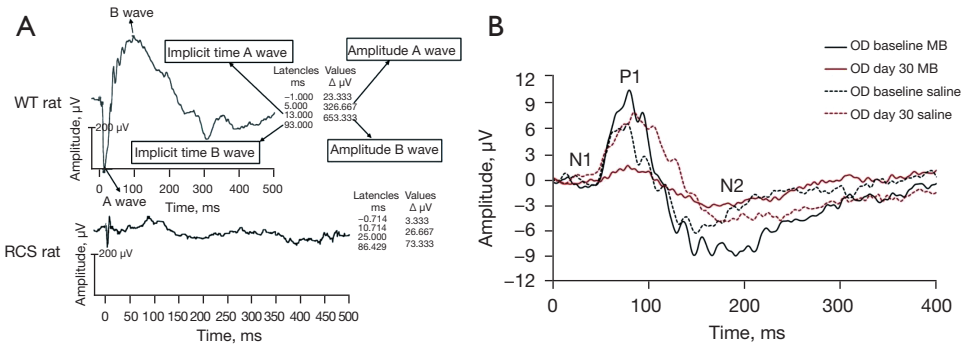

Figure 2 Electrophysiological assessment of retinal function by ERG. (A) Full field scotopic ERG at 39.8 cd*sec/m² flash intensity in WT and RCS rat: at P50 representative ERG waveforms depicted decreased A and B wave amplitude in the RCS rat compared to the WT rat at P50. (B) pERG traces in MB induced glaucoma mouse model, pre and post induction on Day 30 in mice: representative pERG waveforms at baseline (pre) and day 30 (post induction) showed that N1P1 and P1N2 amplitudes are decreased in glaucoma mice compared to the control animals. ERG, electroretinogram; WT, naïve animal; RCS, Royal College of Surgeons; P, postnatal; pERG, pattern ERG; OD, right eye; MB, microbeads.

suprachoroidal routes by performing it immediately after drug delivery (*Figure 1G*). Animals with severe retinal or vitreous hemorrhage, retinal trauma, failed drug delivery (no bleb formation during subretinal delivery), or lens damage on OCT should be excluded and replaced, for the assurance of the consistency in animal's receipt of high-quality injections. With the recent development of OCT-angiography (OCT-A), a non-invasive imaging modality that allows three-dimensional visualization of retinal as well as choroidal vascular structures with higher resolution and accuracy, it is possible to measure the blood flow in the retinal vessels without prior invasive fluorescent dye injection (22).

The ultra-high-resolution AS-OCT provides high-quality images of the tear film, conjunctiva, individual corneal layers, sclera, angle, and lenticular structures of the AS (23). AS-OCT, like posterior segment OCT, is used to characterize AS changes in animal models following treatment, tear film thickness measurement in a dry eye model, and corneal wound healing process in alcohol/alkali/cryo animal models, among other applications (*Figure 1H*).

ERG

ERG is an electrophysiological non-invasive technique commonly used to study retinal function in preclinical ocular animal models. ERG measures the retinal transient electrical potentials in response to light stimulation and responses are divided into component waveforms (a, b and c waveforms). The a-wave, which is the first negative peak, refers to the hyperpolarization of photoreceptors. The b-wave is the first positive peak, which follows the a-wave, and is principally generated by bi-polar and muller cells. The c-wave is a late positive potential after the b-wave, referring to the function of RPE. The implicit time (measured from the stimulus onset to the peak of the waveform in milliseconds, ms) and the amplitude (measured in microvolt, µV) of the a- and b-waves provide insight on the health and function of different types of retinal cells (*Figure 2*). Preclinical animals studies follow the standards of the International Society of Clinical Electrophysiology of Vision (ISCEV) (24) and are incorporate in ERG protocol that follow these recommendations:

(I) Extraction of the rod response to a series weak flash with increasing light intensities, presumably to define the maximal rod-driven waveform;
(II) The mixed (rod-cone) response to a strong flash in the dark-adapted eye;
(III) The definition of oscillatory potentials under light or dark adaptation;
(IV) A response to a strong flash in the light-adapted eye representing a cone signal;
(V) The response to 30 Hz flicker stimulation to identify a cone-driven post-receptoral standing potential.

There are three main types of ERGs technique: full-field flash ERG (ffERG) (*Figure 2A*), pattern ERG (pERG) (*Figure 2B*), and multifocal ERG (mfERG). Each type has different applications and benefits in preclinical studies and used to assess retinal drug toxicity and efficacy of

the treatments that are developed for neurodegenerative diseases (25).

Acknowledgments

I am grateful to Pharmaron, Ocular team members for their critical reading of the manuscript.
Funding: None.

Footnote

Provenance and Peer Review: This article was commissioned by the editorial office, *Annals of Eye Science*. The article did not undergo external peer review.

Conflicts of Interest: The author has completed the ICMJE uniform disclosure form (available at https://aes.amegroups.com/article/view/10.21037/aes-23-6/coif). SK is a current employee of Pharmaron (US) Lab Services. The author has no other conflicts of interest to declare.

Ethical Statement: The author is accountable for all aspects of the work in ensuring that questions related to the accuracy or integrity of any part of the work are appropriately investigated and resolved.

References

1. Negro Silva LF, Li C, de Seadi Pereira PJB, et al. Biochemical and Electroretinographic Characterization of the Minipig Eye in the Context of Drug Safety Investigations. Int J Toxicol 2019;38:415-22.
2. Kaplan HJ. Anatomy and function of the eye. Chem Immunol Allergy 2007;92:4-10.
3. Kumar S, Quach J, Cook N, et al. Characterization and validation of a chronic retinal neovascularization rabbit model by evaluating the efficacy of anti-angiogenic and anti-inflammatory drugs. Int J Ophthalmol 2022;15:15-22.
4. Kumar S, Nakashizuka H, Jones A, et al. Proteolytic Degradation and Inflammation Play Critical Roles in Polypoidal Choroidal Vasculopathy. Am J Pathol 2017;187:2841-57.
5. Kumar S, Berriochoa Z, Ambati BK, et al. Angiographic features of transgenic mice with increased expression of human serine protease HTRA1 in retinal pigment epithelium. Invest Ophthalmol Vis Sci 2014;55:3842-50.
6. Edelman JL, Lutz D, Castro MR. Corticosteroids inhibit VEGF-induced vascular leakage in a rabbit model of blood-retinal and blood-aqueous barrier breakdown. Exp Eye Res 2005;80:249-58.
7. Annear MJ, Mowat FM, Occelli LM, et al. A Comprehensive Study of the Retinal Phenotype of Rpe65-Deficient Dogs. Cells 2021;10:115.
8. Olvera-Montaño O, Baiza-Duran L, Quintana-Hau JD, et al. Comparing The Efficacy Of An Anti-Human VEGF-A Neutralizing Antibody Versus Bevacizumab On A Laser-Induced Choroidal Neovascularization (CNV) Rhesus Monkey Model. Drug Des Devel Ther 2019;13:3813-21.
9. Wang T, Li W, Zhong L, et al. Evaluation of the Effects of Biohcly in an In Vivo Model of Mechanical Wounds in the Rabbit Cornea. J Ocul Pharmacol Ther 2019;35:189-99.
10. Rösch S, Aretzweiler C, Müller F, et al. Evaluation of Retinal Function and Morphology of the Pink-Eyed Royal College of Surgeons (RCS) Rat: A Comparative Study of in Vivo and in Vitro Methods. Curr Eye Res 2017;42:273-81.
11. Wang M, Zhang F, Liu K, et al. Safety evaluation of rabbit eyes on scleral collagen cross-linking by riboflavin and ultraviolet A. Clin Exp Ophthalmol 2015;43:156-63.
12. Tabata H, Shimizu N, Wada Y, et al. Initiation of the optokinetic response (OKR) in mice. J Vis 2010;10:13.1-17.
13. Lu B, Lin Y, Tsai Y, et al. A Subsequent Human Neural Progenitor Transplant into the Degenerate Retina Does Not Compromise Initial Graft Survival or Therapeutic Efficacy. Transl Vis Sci Technol 2015;4:7.
14. Xian B, Zhao M, Peng Y, et al. Fundus photography, fundus fluorescein angiography, and optical coherence tomography of healthy cynomolgus monkey, New Zealand rabbit, Sprague Dawley rat, and BALB/c mouse retinas. Ann Eye Sci 2023;8:10.
15. Ameri H, Chader GJ, Kim JG, et al. The effects of intravitreous bevacizumab on retinal neovascular membrane and normal capillaries in rabbits. Invest Ophthalmol Vis Sci 2007;48:5708-15.
16. LoPinto AJ, Pirie CG, Ayres SL, et al. Comparison of indocyanine green and sodium fluorescein for anterior

segment angiography of ophthalmically normal eyes of goats, sheep, and alpacas performed with a digital single-lens reflex camera adaptor. Am J Vet Res 2017;78:311-20.
17. Duane TD, Tasman W, Jaeger EA. Chapter 4a, Indocyanine Green Angiography. In: Duane's clinical ophthalmology on CD-ROM. Philadelphia, PA, USA: Lippincott Williams & Wilkins; 2002.
18. Alfaro DV. Age-related macular degeneration: a comprehensive textbook. Philadelphia, PA, USA: Lippincott Williams & Wilkins; 2006.
19. Kumar S, Berriochoa Z, Jones AD, et al. Detecting abnormalities in choroidal vasculature in a mouse model of age-related macular degeneration by time-course indocyanine green angiography. J Vis Exp 2014;(84):e51061.
20. Tugal-Tutkun I, Herbort CP, Khairallah M, et al. Scoring of dual fluorescein and ICG inflammatory angiographic signs for the grading of posterior segment inflammation (dual fluorescein and ICG angiographic scoring system for uveitis). Int Ophthalmol 2010;30:539-52.
21. Tugal-Tutkun I, Herbort CP, Khairallah M, et al. Interobserver agreement in scoring of dual fluorescein and ICG inflammatory angiographic signs for the grading of posterior segment inflammation. Ocul Immunol Inflamm 2010;18:385-9.
22. Meyer JH, Larsen PP, Strack C, et al. Optical coherence tomography angiography (OCT-A) in an animal model of laser-induced choroidal neovascularization. Exp Eye Res 2019;184:162-71.
23. Beckmann L, Cai Z, Margolis M, et al. Recent advances in optical coherence tomography for anterior segment imaging in small animals and their clinical implications. Ocul Surf 2022;26:222-33.
24. Robson AG, Nilsson J, Li S, et al. ISCEV guide to visual electrodiagnostic procedures. Doc Ophthalmol 2018;136:1-26.
25. Pasmanter N, Petersen-Jones SM. A review of electroretinography waveforms and models and their application in the dog. Vet Ophthalmol 2020;23:418-35.

doi: 10.21037/aes-23-6
Cite this article as: Kumar S. Fundus photography, fluorescein angiography, optical coherence tomography and electroretinography of preclinical animal models of ocular diseases. Ann Eye Sci 2023;8:8.